SEISMIC ASSESSMENT OF FREE-STANDING ARTEFACTS: FULL-SCALE TESTS ON LARGE SHAKE TABLE

Luisa Berto[(1)]* – Luigi Di Sarno[(2, 3)] – Michalis Fragiadakis[(4)] – Irene Rocca[(1)] – Anna Saetta[(1,5)]

[(1)]DCP – University IUAV of Venice, Campus Terese, Dorsoduro 2206, 30123 Venezia – Italy

[(2)]DIST – University of Naples Federico II, via Claudio, 21, 80125, Naples, Italy

[(3)]Institute for Risk and Uncertainty, School of Engineering, University of Liverpool, L69 3GQ, Liverpool, UK

[(4)]NTUA - National Technical University of Athens, Iroon Polytechniou str 15772 Zografou, Greece

[(5)]Associate to National Research Council (CNR), Institute for Construction Technologies (ITC), Italy

**Corresponding Author: e-mail: lberto@iuav.it*

Abstract

Recent severe earthquakes highlighted the high vulnerability of artistic assets. Thus, the seismic assessment and formulation of preservation strategies of artefacts are key challenges of modern earthquake engineering, which require theoretical and experimental investigations. The present paper discusses the outcomes from large scale shake table tests carried out on full-scale free-standing artefacts. The study is also aimed at evaluating the reliability of existing simplified formulations to predict the rocking motion activation. Emphasis is on prototypes of marble busts with solid and hollow pedestals with different geometries. Comprehensive tests were performed within "Seismic Resilience of Museum Contents" (SEREME) project, which was recently funded by H2020 Framework Programme - Seismology and Earthquake Engineering Research Infrastructure Alliance for Europe (SERA). Uniaxial and biaxial earthquake natural records with different amplitudes and frequency contents were considered to assess the rocking motion of the sample specimens. Response parameters such as uplift, horizontal and vertical accelerations, angular velocity were measured to assess the rocking response of the sample freestanding busts and pedestals. Coefficients of amplification (CAF) of acceleration were also computed. The value of CAF showed that for solid pedestals they were not significantly influenced by peak ground acceleration (PGA) and earthquake type. Conversely, hollow pedestals, which were characterized by larger values of CAF than solid counterparts, ranging between 1 and 7, were affected by PGA and earthquake characteristics. Finally, the outcomes of the presented shake table tests showed that uplifts and angular velocity are effective measures for assessing rocking occurrence of tested artefacts.

Keywords: artistic assets; rocking; shake table tests; vulnerability; simplified methods; seismic assessment.

1 Introduction

The seismic safety of art collections has received in recent years increasing attention from public and scientific communities due to their enormous economic and cultural relevance and consequences. Vulnerability assessment methods and risk mitigation strategies are thus needed to ensure seismic resilience of museum contents (e.g. [1] - [7]).

Building contents can be either attached to the structure or consist of elements that are simply standing; for museum artefacts, most of them are free-standing components. The seismic assessment of such artefacts, especially busts and slender human-shape statues, includes the dynamic response of rocking rigid blocks. Rocking systems possess remarkable stability against seismic loading despite the lack of a lateral load resisting mechanism (e.g. [8] - [10]). The behaviour of freestanding rigid bodies subjected to horizontal ground acceleration is inherently complex and characterized by nonlinear dynamics. Thus, it has been extensively studied in the last two decades. The seminal analytical work by Housner [11] carried out on the seismic response of rocking objects dates back to the early 60's. The latter pioneering work stimulated several quantitative studies that have focused primarily on numerical solutions, e.g. [12] - [20], among others. These numerical studies demonstrated high sensitivity of the rocking response to small changes in geometry of free-standing elements, boundary conditions and input seismic motions. Rocking motion was also found strongly influenced by the type and the frequency of earthquake excitation, thus conforming findings of previous research (e.g. [21] – [24). In most of numerical simulations carried out in the aforementioned studies, friction coefficient is assumed high enough to prevent sliding between the rigid block and the horizontal surface of the floor; thus, a significant simplification follows in the formulation. If the unanchored block and architectural finishes used for the floor ensures the assumptions of rigidity and no-sliding, then rocking response is controlled primarily by geometric parameters. Thus, in no-sliding conditions, the approach based on West's formula ([25]) can be efficiently adopted to estimate the minimum horizontal acceleration for rocking initiation. The latter motion is triggered when the inertial forces, which are induced on the rigid block by the horizontal strong motions, overcome the effects of gravity loads.

Following the early experimental tests by Milne and Omori [26] and Kirkpatrick [27], in recent years, many experimental programs were carried out to investigate stability of rocking blocks, thus aiming at formulations of approaches to predict rocking response and the associated overturning risks. Experimental evidence obtained from shake-table tests can contribute significantly to the advances of knowledge for the seismic assessment of free-standing components, especially artistic assets. Purvance et al. [28] used experimental results from shake-tables to investigate the overturning response of symmetric and asymmetric blocks with both simple and complex contact conditions at the base of the free-standing components. The outcomes of such experimental tests and numerical simulations were used for the derivation of seismic fragility relationships for block overturning. Three boulders incorporating jagged bases were tested on a shake table to the point of overturning. It was found that such boulders overturned at lower accelerations than geometrically similar counterparts with flatter interfaces. A further comprehensive experimental testing program was carried out by Konstantinidis and Makris [29] on full-scale freestanding laboratory equipment which were assumed to be located on several floor levels of building structure. The test results were utilized to derive ready-to-use fragility curves. It is worth noting that, when the building contents are located at higher floor levels, specific approaches have to be applied, e.g. Berto et al. [30], Petrone et al. [31], Rodriguez et al. [32].

Kafle et al. [33] carried out an extensive experimental program on the response of rigid blocks. Free-standing components were subjected to seven earthquake time histories using the peak displacement demand as the main intensity measure. Earthquake scenarios were generated by stochastic simulation. Fragility curves were derived analytically and then compared to the experimental results. Similar approaches for assessing experimentally typical freestanding building contents were also adopted by Petrone et al. [34], Berto et al. [35], Di Sarno et al. [36] and D'Angela et al. [37]. Additional shake-table tests carried out by Berto et al. [38] provided experimental evidence that rocking may occur for acceleration lower than the value generally assumed as the rocking limit, which is proportional, by acceleration gravity, to the aspect ratio. A different threshold value of acceleration was proposed to define a safe acceleration limit for seismic vulnerability assessment of free-standing elements. Such limit accounts for the real conditions of rocking behaviour, e.g. element imperfections, not perfectly rigid conditions for both block and supporting floor, not planarity of the contact surfaces.

While a number of studies have analyzed the response of the single rocking block, very few have tested the response of multiple block systems subjected to earthquakes. The experimental work of Wittich and Hutchinson [39] studied asymmetric dual-block free-standing component configurations. It is found that, for rocking rigid objects, such as artefacts, the response can be size-dependent, thus the scaling of the specimens is not possible and the experimental tests should be based on full-scale specimens. The shake table tests indicated that, for dual-block systems, the presence of a pedestal increases the likelihood of collapse and amplitude of rocking demands, in general. However, certain geometric and interface combinations yield a more stable top block (also named "tower") in a dual-body configuration compared to a single-body configuration, because of the dependence of the pedestal response on the geometry of the tower. Irregular free-standing dual-blocks subjected to earthquake motions were also studied experimentally and numerically by Arredondo et al. [40], Al Abadi et al. [41], Khalid

et al. [42] and Anagnostopoulos et al [43]. Experimental shaking-table tests were carried out on modular prototypes, which allow the replication of representative mass distributions, sizes, and/or slenderness ratios for typical objects. The tests were used to calibrate the numerical model. It was found that the dynamic behavior under irregular conditions (asymmetrical shape and/or non-uniform mass distribution) can be estimated with the appropriate geometric and density considerations. The rocking response of irregular objects can be highly influenced by the level of eccentricity of the object when excited by motions with high displacement amplitudes, while such influence was not found noticeable by wider objects. In both studies, peak displacement parameter of the supporting floor's motion was assumed as Intensity Measure (IM) for the seismic performance-based assessment of the free-standing components.

The above discussion highlighted the lack of robust methods to predict the rocking response and the need to use combinations of IM such as peak ground acceleration (PGA) peak ground velocity (PGV), and their ratio PGV/PGA, as also discussed by Casapulla et al. [44].
The present paper illustrates the outcomes of recent comprehensive tests carried out on the shake-table to assess the response of museum artefacts consisting of pedestals (solid and hollow) and busts. Uniaxial and biaxial earthquake input motions with different amplitudes and frequency contents were considered to evaluate and discuss the rocking motion activation, considering the existing simplified prediction formulations. Several response parameters were investigated. The outcomes of the comprehensive shake table tests carried out by using earthquake ground motions with different frequency content showed that uplifts and angular velocity are effective measures for assessing rocking occurrence of tested artefacts.

2 Experimental testing program

2.1 Description of experimental research

The aim of the comprehensive experimental research program summarized in this section is to investigate the seismic response of typical museum sculptures (statues and busts) and evaluate the performance of novel and cost-effective risk mitigation devices to ensure the seismic resilience of museum contents. The experimental tests were carried out on the AZALEE 6-DOFs seismic simulator of Commissariat à l'Energie Atomique (CEA) in Saclay, Paris. Such tests were carried out as part of the project Seismic Resilience of Museum Contents (SEREME), funded by "Seismology and Earthquake Engineering Research Infrastructure Alliance for Europe" (H2020-INFRAIA SERA project, [45]).
The full-scale busts and statues were selected with different geometry and weights; all specimens are made of solid marble. They represent replicas of three ancient emperors, i.e. Traianus, Augustus, and Titus, and two typical female-shaped statues: a sample standing on a low-height marble pedestal and a female statue without pedestal. To reproduce realistic conditions in most of the museums worldwide, the busts were positioned on pedestals. Based on an extensive survey, the selected pedestals have adequate height to bring the specimen up to the "eye-level". Two different traditional pedestals were adopted for the experimental tests: solid pedestal (S/P), and hollow pedestal (H/P). In addition, a modern metallic pedestal, provided by an Italian manufacturer, was considered.
The present paper focuses on the response assessment of the busts tested on the traditional pedestals, Figure 1. In particular, the case of the Augustus bust (B) on solid pedestal is deeply investigated. Comparisons with the case of the bust on the hollow pedestal are also carried out to estimate the effects of the weight and slenderness of the support on the response of the bust. The traditional pedestals were made of concrete, to replicate the specific weight of marble counterparts. Solid pedestal has larger weight (about 500kg) and base; hollow pedestal is slender and lighter (226kg); its base has also a smaller width. All the pedestals have 3-cm thick marble plates on the upper and the lower faces, to reproduce realistic conditions for in-situ/in-museum friction. The pedestals were, in turn, mounted (without connections) on marble floor, which is bolted on the shake table. Additional details on the SEREME research program can be found in Fragiadakis et al. [46].
The friction coefficient μ between the interface of pedestals and floor as well as pedestals and the base of the busts is a critical parameter for the assessment of the dynamic response of the specimens (e.g. [11]; [22]; [47], [48]; among others). Friction coefficients evaluated experimentally may have a large range of variation ([49; [50]): laboratory test reports provide values from 0.4 to 0.8 for marble-marble interface. The static friction coefficient for marble-marble interface was measured during the SEREME tests at CEA. The inclined tests were repeated 10 times to determine the mean friction angle. For the pedestal-plate on shaking table marble interface, the mean friction coefficient μ=0.79 was evaluated, while for the bust-pedestal interface a coefficient μ=0.39 was estimated. Thus, to prevent the effects of friction coefficients, a thin layer of a rubber material was glued at the bottom of the busts. Such measure was effective in eliminating sliding during the tests and preventing additional slight rocking/wobbling, as detected in previous experimental tests carried out by Wittich and Hutchinson [50].
To evaluate the influence of frequency contents and directionality of seismic ground motions, the configurations were experimentally tested using different uniaxial, biaxial and triaxial earthquake records at increasing amplitudes, thus performing an experimental dynamic analysis. Four different seismic records were considered, as further discussed in Section 2.4.

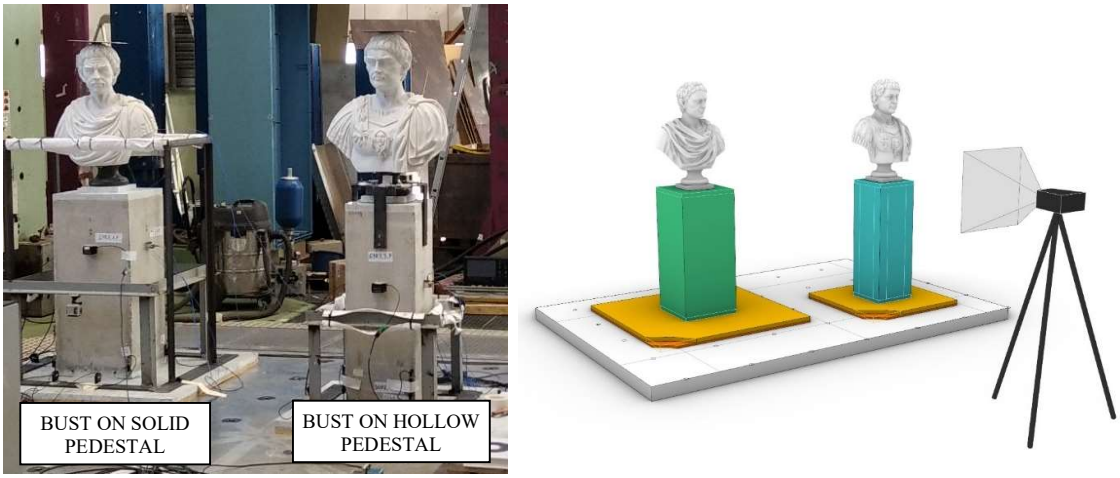

(a) (b)

Figure 1. Test configuration assessed in the present paper: (a) busts on solid and hollow pedestal and (b) position of the high-resolution camera.

2.2 Geometric survey and model characterization

A three-dimensional (3D digital model) was created for the tested specimens using a highly accurate 3D survey carried out with a laser scanner Faro® Focus 3D Cam2, [51]. The aim of the survey is to (i) determine the fundamental geometrical and mass properties of the artifact useful for the stability analysis, namely center of gravity (CG) position, rotational moments of inertia, and (ii) define the finite element model (FEM) for numerical simulations, which required thorough mesh analysis and optimization. Figure 2 provides the photo (a), the 3D digital model (b), and the implemented FEM model (c) for the Augustus bust.

(a) (b) (c)

Figure 2. Emperor Augustus bust: (a) photo;(b) 3D digital model; (c) FEM model.

The position of CG and the geometric characteristics of the bust and pedestal are provided in Figure 3. The pedestal is a concrete solid prism with squared base (side = 450 mm; total height = 1010 mm).
The hollow pedestal, for which some results will be reported in the following for the sake of comparison, is a parallelepiped with squared base of side 350 mm, total height 1010 mm and thickness 80 mm, with a weight less than half that of the solid counterpart.

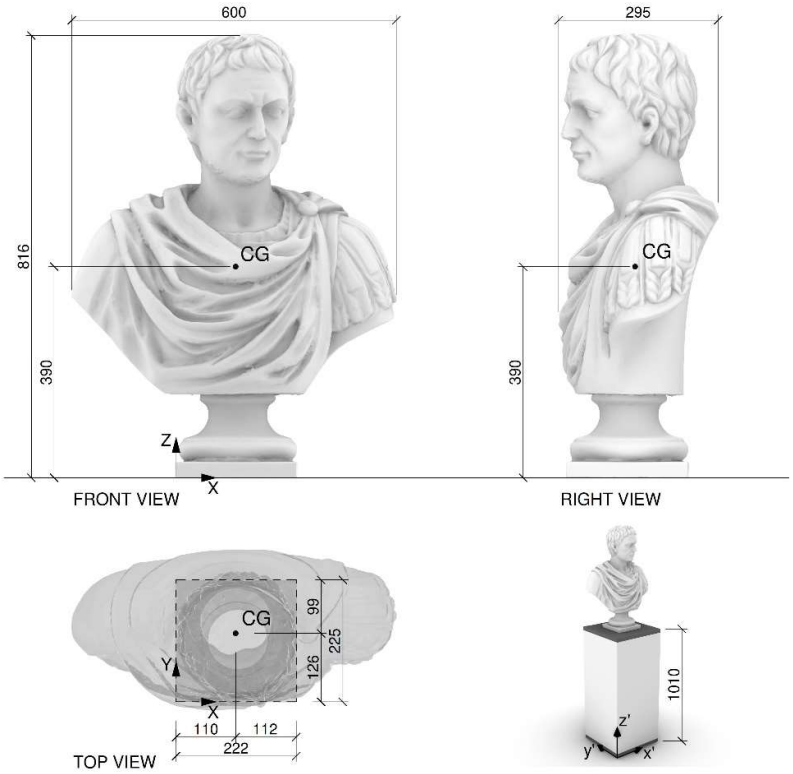

Figure 3. Emperor Augustus bust: main geometrical characteristics and centre of gravity position with indication of reference system

Utilizing the 3D digital model, geometric and inertial parameters were computed. Table 1 summarizes such parameters computed for the bust, the two pedestals and the system bust/pedestal, which corresponds to an ideal condition of bust firmly connected to the pedestal like a single body.
In detail, the table reports the weight (W), the height (H) of CG and, for X- and Y-direction, the aspect ratio (B/H), the inertial radius (i) and the semi-diagonal dimension ($r = \sqrt{B^2 + H^2}$), where B is the minimum distance between the base edge around which the oscillation occurs and the projection of the center of gravity (CG). As an example, for the bust, B is equal to 110 mm and 99 mm respectively along X- and Y-direction (Figure 3).

Table 1. Geometric and inertial parameters for Augustus bust (B), solid (S/P) and hollow (H/P) pedestals, bust/solid pedestal (B+S/P), bust/hollow pedestal (B+H/P).

	W (kN)	**H (mm)**	**$B_{X,min}/H$**	**$B_{Y,min}/H$**	**i_X (mm)**	**i_Y (mm)**	**r_X (mm)**	**r_Y (mm)**
B	1.070	389.6	0.283	0.253	205.1	223.2	404.9	409.6
S/P	5.113	505.0	0.446	0.446	300.8	300.8	548.3	548.3
H/P	2.182	505.0	0.347	0.347	294.7	294.7	530.0	530.0
B + S/P	6.183	656.6	0.342	0.340	443.9	445.3	693.9	693.4
B + H/P	3.252	793.3	0.220	0.216	499.5	501.8	812.2	811.5

2.3 Instrumentation used for the shaking table tests of the specimens

The motion of the specimens was recorded during the shake table tests using accelerometers, gyroscopes and displacement sensors. The properties of the instruments are summarized in Table 2.

Table 2. Instrumentations used to monitor the specimens during the shake table tests.

Instrument	Sensor Type	Measured Response Parameter	Properties
LVDT	Penny & Giles SLS 130-0050-L-50-01-N	Displacement for pedestal uplift	50 mm stroke and 10 Volts input
LVDT (wire)	Firstmark 175-0401-L3D	Lateral displacement for pedestal	127 mm stroke and 5 Volts input
Gyroscope	Sensorex SX43600	Angular velocity of the pedestal	Velocity range ± 200 °/s and 1 Volt input
Gyroscope	DTS ARS-300	Angular velocity of the bust	Velocity range ± 300 °/s and 5 Volts input
Accelerometers	PCB 3711D1FA20G	Horizontal and vertical accelerations (pedestal and bust)	Maximum acceleration 30g and 10 Volts input

All the data measured during the experimental tests were recorded with a sampling rate of 512 Hz and a lowpass filter with a cut off frequency of 150 Hz.
The location of the instrumentation used for the tests is shown in Figure 4.

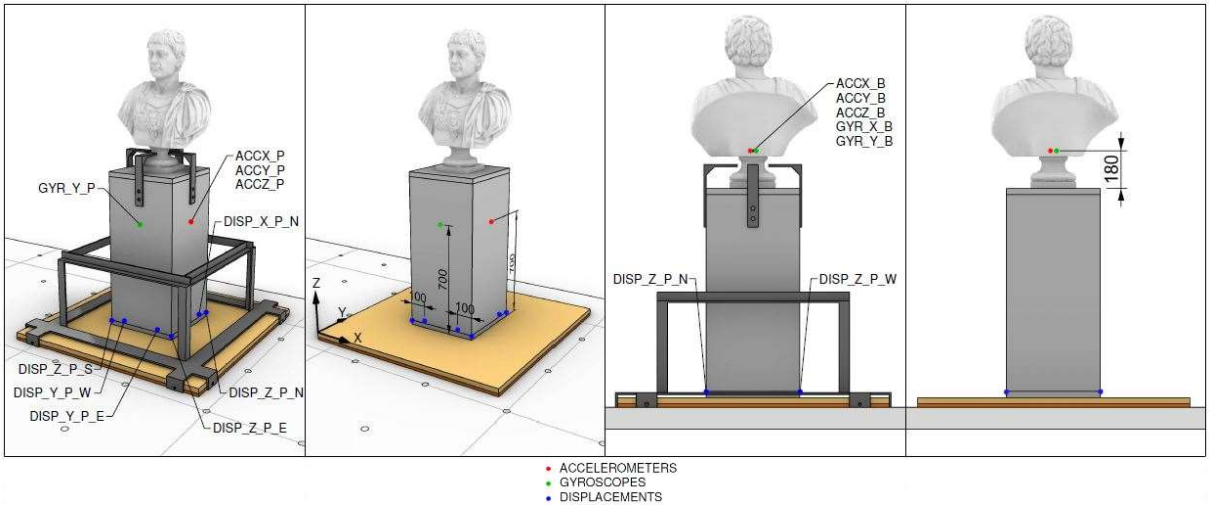

Figure 4. Instrumentation on the solid pedestal and on the Augustus bust (dimensions in mm)

2.4 Ground motions selected for the testing

Four natural records were considered for the tests carried out on the shake table at CEA, Saclay. Such records were selected from historical near-field earthquakes that occurred in Greece (Kalamata, 1986 and Athens, 1999) and Italy (L'Aquila, 2009 and Emilia, 2012); the earthquakes have moment magnitude M_w ranging between 5.9 (Athens, 1999) and 6.3 (L'Aquila, 2009). Most of the ground motions were registered on stiff soil as further detailed in Table 3. The elastic response spectra of these ground motions are depicted in Figure 5.

Table 3. Ground motion records used for the shaking table tests. (L=Longitudinal; T=Transverse)

Earthquake	Date	Mw	Station	Distance hypocentral (km)	Soil category	PGA (g)	PGV/PGA m/(sg)
Emilia, Italy	29.05.2012	6.0	T0800	14.4	C* (EC8)	L: 0.33 T: 0.25	0.83 0.80
Athens, Greece	07.09.1999	5.9	Syntagma Metro B	10.0	Stiff soil	L: 0.11	0.89
L'Aquila, Italy	06.04.2009	6.3	Aterno river-AQA	< 2.0	Stiff soil	L: 0.45	0.55
Kalamata, Greece	09.13.1986	6.2	Nomarchia	5.0	Stiff soil	L: 0.22	1.59

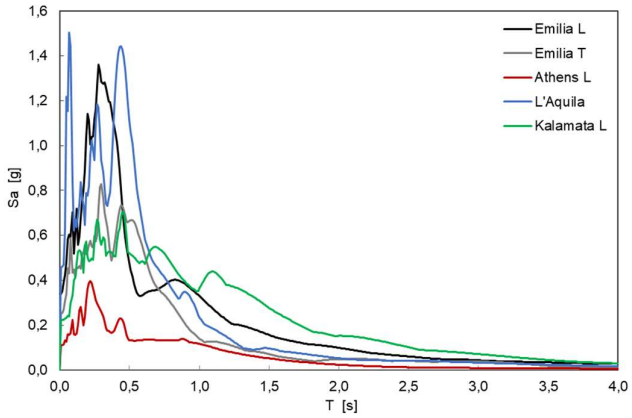

Figure 5. Acceleration response spectra of ground motions (5% damping)

The PGV/PGA ratio has a strong correlation with the peak input energy of ground motion (e.g. [52]; [53];[24] among others). Strong motions with low PGV/PGA values have significant contribution for earthquake vibrations in the short period range. On the other hand, high values of PGV/PGA, e.g. greater than 1.25 $ms^{-1}g^{-1}$ generate remarkable effects in the long period range (low predominant frequencies); they also exhibit broader response spectra and longer duration. To assess the dynamic response of rigid blocks, single and multiple, under different seismic loading scenarios, accelerograms with both low and high PGV/PGA ratios were considered for the shake table tests.

2.5 Test matrix

Table 4 presents the test matrix with the sequence of the uniaxial tests carried out in the configuration including Augustus bust and solid pedestal (S/P+B), which is the focus of this paper, as mentioned in Section 2.1. For each test, the table summarizes the type of earthquake used, the test label, the input PGA recorded on the table, the scaling factor and the type of tested specimen, i.e. pedestal with or without bust. For completeness also the type of tested specimen for hollow pedestal is reported. It is worth noting that in some tests the pedestals were tested alone to determine the dynamic response of the one-block system.

Table 4. Test matrix of the inputs for Augustus bust (B), solid pedestal (S/P) and hollow pedestal (H/P)

Signal	Test Label	PGA (g)	Scaling factor	Tested Specimen	
Emilia L in X direction (Emilia-L_X)	401_EM_X	0.24	0.73	S/P + B	H/P + B
	402_EM_X	0.34	1.03	S/P + B	H/P + B
	407_EM_X	0.41	0.94	S/P + B	H/P + B
	412_EM_X	0.47	1.42	S/P + B	H/P
	446_EM_X	0.48	1.45	S/P	H/P + B
Emilia L in Y direction (Emilia-L_Y)	408_EM_Y	0.20	0.80	S/P + B	H/P + B
	410_EM_Y	0.30	1.20	S/P + B	H/P + B
	411_EM_Y	0.39	1.56	S/P + B	H/P + B
Emilia L in X direction + Emilia L in Y direction	414_EM_XY	0.34 0.25	1.06 0.96	S/P + B	H/P + B
Athens L in X direction (Athens-L_X)	427_AT_X	0.20	1.82	S/P	H/P + B
	428_AT_X	0.28	2.55	S/P	H/P + B
	429_AT_X	0.43	3.91	S/P	H/P + B
	445_AT_X	0.47	4.27	S/P	H/P + B

L'Aquila L in X direction (L'Aquila-L_X)	436_AQ_X	0.21	0.47	S/P	H/P + B
	437_AQ_X	0.23	0.51	S/P	H/P + B
	438_AQ_X	0.27	0.60	S/P	H/P + B
	439_AQ_X	0.33	0.73	S/P	H/P + B
	441_AQ_X	0.35	0.78	S/P	H/P + B
Kalamata L in X direction (Kalamata-L_X)	423_KA_X	0.15	0.68	S/P + B	H/P + B
	424_KA_X	0.15	0.70	S/P + B	H/P + B
	425_KA_X	0.25	1.14	S/P + B	H/P + B
	426_KA_X	0.30	1.36	S/P + B	H/P + B

3 Experimental Results and Discussion

3.1 Observed dynamic response

Visual observations during the tests are first presented, then the measured response parameters recorded by instruments are discussed. Emphasis is on the significant parts of the waveforms, i.e. those waveform parts of the records that affect the rocking initiation of the busts and/or pedestals. The significant part of the waveforms is assumed as the part of the signal that shows a drop of 70% with respect to the peak of acceleration of the whole signal. For example, for the case of the Emilia L in X-direction and Kalamata L in X-direction records, Figure 6 highlights the significant part of the horizontal strong motion measured on the shake table.

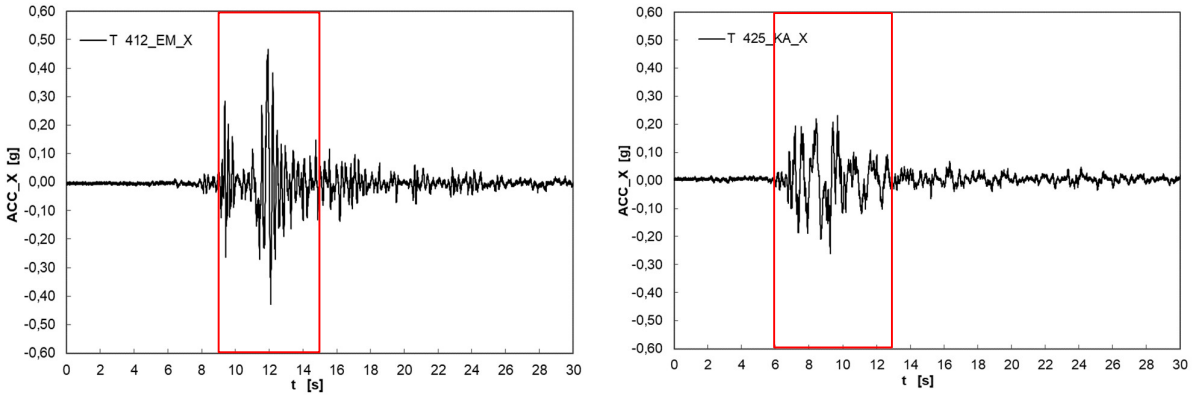

(a) (b)

Figure 6. Horizontal acceleration of the table with indication of the significant part: (a) 412_EM_X (b) 425_KA_X

The earthquake time history response analysis carried out in the following section shows the relevance to investigate, through the time-stepping approach, the occurrence of relevant response parameters (horizontal/vertical acceleration, angular velocity and uplift) measured on the pedestal and bust.

3.1.1 Visual observations

Detailed visual observations were carried out through a high-resolution camera, which was located close to the shake table, as displayed in Figure 1b. In all tests the solid pedestal seems to be at rest. Table 5 summarises the results for each shake table test carried out on busts. For rocking mode, the occurrence time and the corresponding value of input PGA and PGV for its initiation and, in case, for its steady response are also reported. For overturning, (test 426_KA_X), the maximum values of PGA and PGV are not synchronous with the overturning time occurrence (t_o = 10s), so these values with their relative occurrence time are also reported.

Table 5. Results of visual observations for Augustus bust

Signal	Test Label	Behaviour	Rocking Initiation	Steady Response
			Occurrence time, PGA, PGV	Occurrence time, PGA, PGV

Emilia-L_X	401_EM_X	N		
	402_EM_X	R	11.9s, 0.33g, 0.19m/s	
	407_EM_X	R	9.4s, 0.23g, 0.08m/s	
	412_EM_X	R*	9.4s, 0.26g, 0.09m/s	11.9s, 0.46g, 0.32m/s
Emilia-L_Y	408_EM_Y	N		
	410_EM_Y	N		
	411_EM_Y	N		
Emilia-L_X + Emilia-T_X	414_EM_XY	R*	9.5s, 0.15g, 0.06m/s	11.9s, 0.30g, 0.18m/s
Kalamata L_X	423_KA_X	N		
	424_KA_X	R	7.3s, 0.15g, 0.84m/s	
	425_KA_X	N		
	426_KA_X	R*	7.2s, 0.24g, 0.08m/s	8.4s, 0.27g, 0.25m/s
		O		10s, 0.15g, 0.13m/s 8.7s, 0.30g, 0.43m/s (max)

Keys: N = Nothing; R = Rocking initiated/triggered and quickly damped; R*= Fully developed and persistent rocking, rocking with several well recognizable oscillations of the artifact; O = Overturning.

3.1.2 Assessment of time-history response

Horizontal accelerations and angular velocity of pedestals and busts, vertical displacements and accelerations of the pedestals are measured and discussed hereafter for unidirectional and bidirectional ground motions. The outcomes for Emilia and Kalamata earthquakes are reported to investigate the influence of different frequency contents on the response of bust and pedestals.

Response under uniaxial loading

The effects of uniaxial loading are discussed with reference to two tests carried out with Emilia-L_X record with similar PGAs, namely 412_EM_X (PGA=0.47g) and 446_EM_X (PGA=0.48g), and one test with Kalamata-L_X record, namely 426_KA_X (PGA=0.30g).

Figure 7 reports the acceleration (horizontal and vertical) and angular velocity response of the pedestal and bust during the test 412_EM_X, besides the vertical displacement of the pedestal. The horizontal accelerations measured at the shake table level are compared in Figure 7a with those registered on the pedestal and bust. As above mentioned, the time history refers to the ground motion time-windows with significant horizontal accelerations, namely values larger than 0.15g. Two strong motion bands can be identified in the time history on the shake table, as illustrated in Figure 7a. The first mainshock (between 9s and 11s), in the following 1st shock, exhibits 2-seconds duration and possesses a single cycle with acceleration amplitude exceeding 0.20g. The second and more significant mainshock, in the following 2nd shock, has longer duration (4 seconds, i.e. between 11s and 15s) and comprises three cycles with accelerations higher than 0.20g. The maximum acceleration of the second shock is 0.47g, which is nearly 70% larger of the PGA of the first shock. As shown in Figure 8, the Fast Fourier Transform (FFT) of the horizontal input acceleration time history has significant amplifications in the range of 3.0-12.0 Hz for the first shock. For the second shock, the amplification in the FFT is between 0.5 and 5.0 Hz. For both shocks the peaks of the accelerations are at frequencies between 3.5 and 4.0 Hz. Higher demand is imposed by the second shock at lower frequencies (0.5-5.0 Hz versus 3.0-12.0 Hz).

Figure 7a and Figure 8 indicate a substantial mismatch between the signal on table and pedestal, and the response recorded on the bust, both for the time-histories and FFT spectra. For the 1st shock such mismatch is significant at about 9.4s, thus leading to the onset of incipient rocking of the bust on the solid pedestal. The latter behaviour is also found in the angular velocity and vertical accelerations which are displayed in Figure 7b-c. For the 2nd shock, measurements from the gyroscope in Figure 7b highlight the onset of the bust rocking motion at 11.8s, which is close to the peak of table accelerations reported in Figure 7a. For 2nd shock, the presence of long period (short frequency) bust response at about 2.0 Hz as per Figure 8, shows the occurrence of a fully developed rocking, in accordance with the visual observations. Such response is also confirmed by the angular velocity and vertical acceleration time-histories provided in Figure 7b-c. The bust continues its sway oscillations even after the ground motion ceases. Moreover, a bust rocking period in the range 0.3-0.5s can be visually identified from Figure 7a.

The rocking mode corresponds to the amplification in the FFT spectrum between 2.0 and 3.0Hz (Figure 8). This finding is also confirmed by the time history of gyroscope in Figure 7b which shows a bust oscillation period corresponding to a frequency at about 2Hz.

As far as the solid pedestal response is concerned, Figure 7a and Figure 8 indicate a close match between the pedestal response and the shaking table input. The FFT curves are superimposed, for 1st shock, up to about 15Hz.

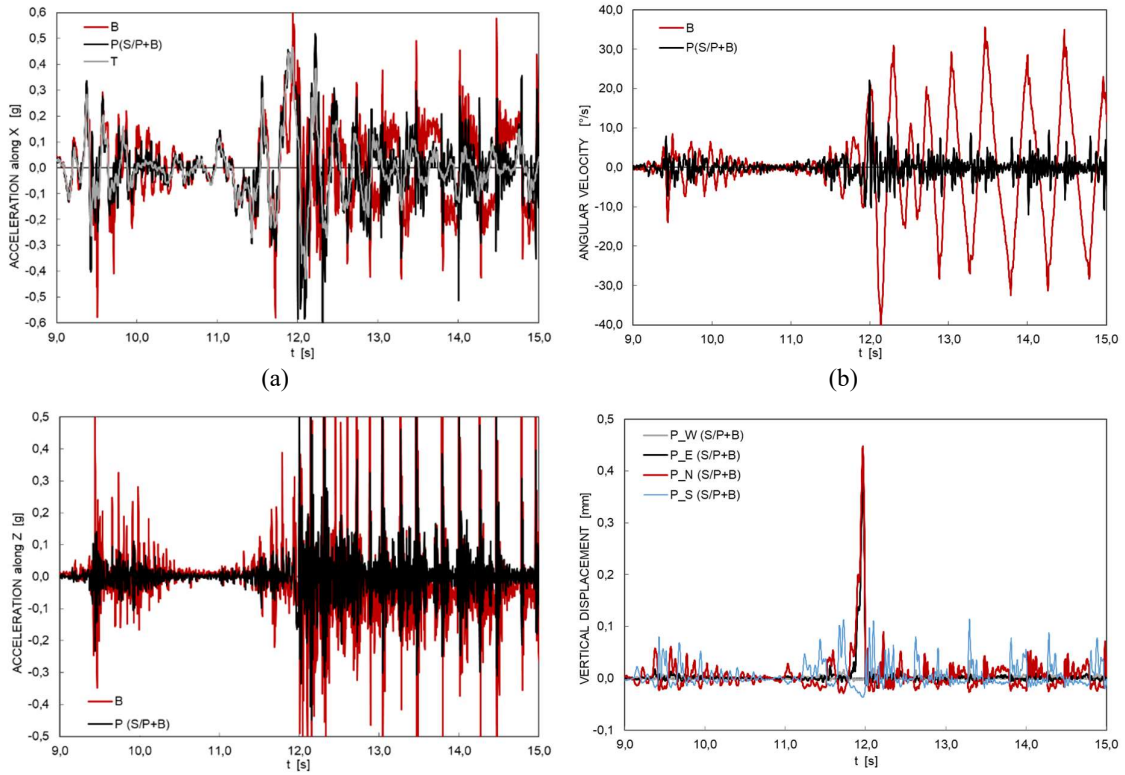

Figure 7. Test 412_EM_X. (a) horizontal acceleration: shaking table (ACCTX), solid pedestal (ACCX_P (S/P+B)), and bust on solid pedestal (ACCX_B); (b) angular velocity: solid pedestal (GYRY_P (S/P+B)) and bust on solid pedestal (GYRY_B); (c) vertical acceleration: solid pedestal ACCZ_P (S/P+B)) and bust on solid pedestal (ACCZ_B); (d) vertical displacement of solid pedestal DISPZ_P (S/P+B)).

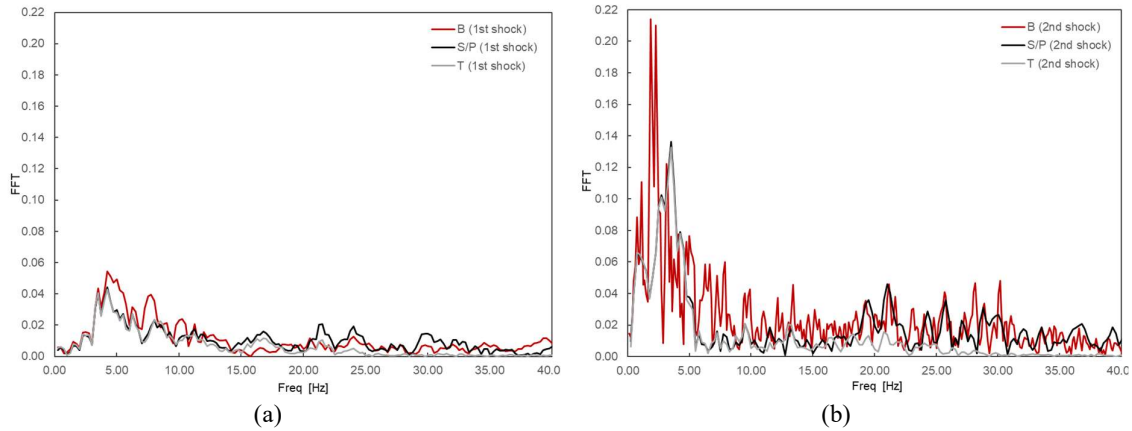

Figure 8. Fast Fourier Transform for the horizontal acceleration signal on shake table (T), solid pedestal (S/P) and bust (B) for test 412_EM_X: (a) 1st shock (b) 2nd shock

Nonetheless, from the time history responses in Figure 7, a pedestal wobbling without significant uplift on the edges is observed at about 9.5s. Such behaviour, which was detected also from the measurements of the gyroscope and the vertical accelerometers, is also confirmed by the LVDT time history in Figure 7d. This response mode

may be generated by imperfections at the base of the pedestal, thus confirming the findings in Wittich et al. [50] and Berto et al. [38]. For the 2nd shock, when the table peak acceleration is reached (i.e. at 11.9s), the onset of slight rocking is detected by the different amplitudes of the acceleration of the shake table and pedestal in Figure 7a. The vertical displacements, Figure 7d, demonstrate that the solid pedestal initiates the uplift for rocking at about 11.8s but without establishing a fully developed rocking motion.

To investigate the effects of the weight and slenderness of pedestals without bust on the initiation of rocking, experimental earthquake response of solid and hollow pedestals when subjected to two tests carried out with Emilia-L_X record with similar PGAs (test 412_EM_X and test 446_EM_X) is compared.

From visual observation of these tests, the H/P shows a developed rocking mode, while the S/P seems to remain at rest, as above mentioned for all tests. Figure 9 compares the results of hollow pedestal alone (test 412_EM_X) with the ones of solid pedestal alone (test 446_EM_X).

Horizontal accelerations of the hollow pedestal are much larger than those used as input on the shake table (see Figure 9b), especially when the PGA=0.47g, at about 11.9 seconds. This is not the case for the solid pedestal, as seen in Figure 9a. The maximum response of the hollow pedestal is not synchronous with the peak values of the input motion on the shake table. The amplifications of horizontal accelerations are higher than 3.5 as further discussed in Section 3.2. Such response is found for both shocks. Higher values of PGAs on the shake table during the second shock (values greater than 0.40g) generate rocking oscillations for the hollow pedestal as proved by the values of angular velocity, Figure 9c.

The rocking response for the hollow pedestal is also detected in the vertical acceleration time history, where several impacts are recorded, and in the vertical displacements measured by LVDT as per Figure 9d. Uplifts started at about 12s corresponding to the peak of acceleration. The peaks of vertical displacements (uplift of 10mm) and the maximum angular velocity (30°/s) are synchronous; these values are significantly higher than those measured for the solid pedestal, i.e. 0.10 mm and 8.3°/s respectively.

For the solid pedestal alone, test 446_EM_X, the acceleration response (Figure 9a), matches the shake table strong motion; however, the presence of high frequencies is also detected. In the 2nd shock only, at about 11.9 seconds, the angular velocity (Figure 9c), vertical acceleration and LVDT response history (Figure 9d) reveal multiple low peaks. The latter response corresponds to clearly developed wobbling.

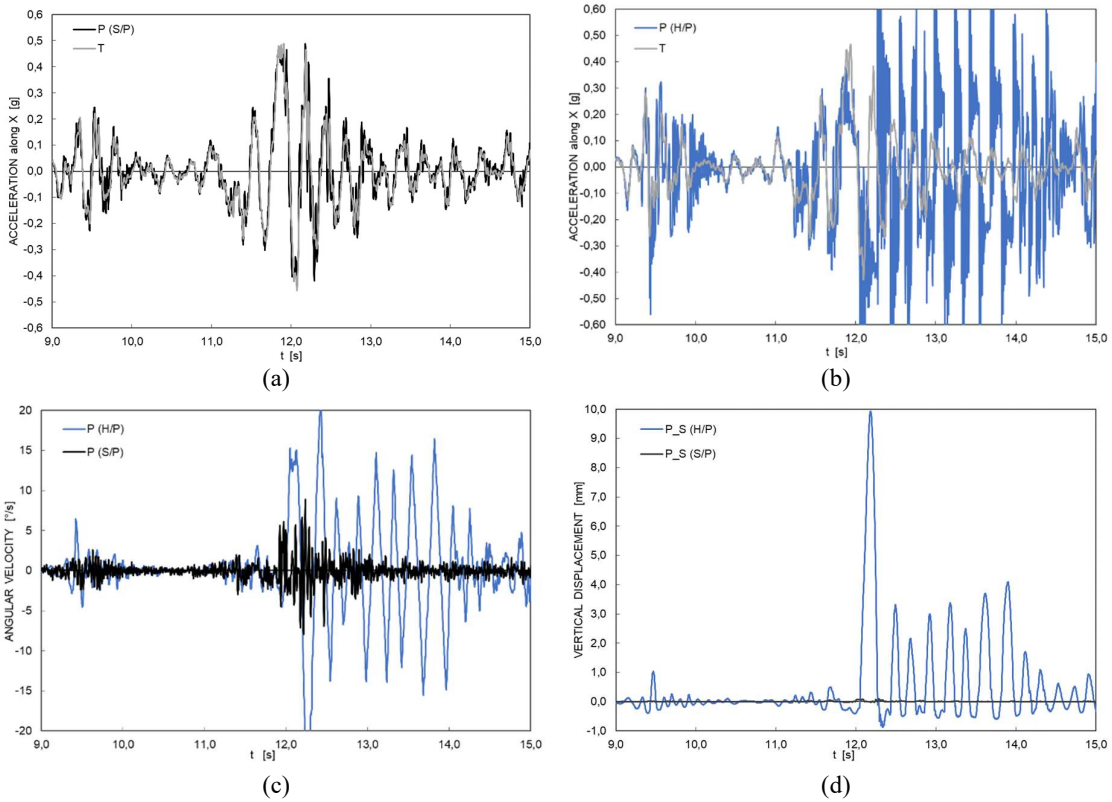

Figure 9. Solid pedestal and hollow pedestal without bust, with input EM_X with close PGA value (a) Test 446_EM_X: horizontal acceleration of shaking table and of solid pedestal. (b) Test 412_EM_X: horizontal acceleration of shaking table and of hollow pedestal. (c) Angular velocity comparison: hollow pedestal in 412_EM_X and solid pedestal in 446_EM_X. (d) Vertical displacement comparison: hollow pedestal in 412_EM_X and solid pedestal in 446_EM_X.

When the effects of frequency contents are considered, the response of the hollow pedestal differs significantly from that of the ground motion in the range of low frequencies. For the solid pedestal, there are differences only in high frequencies range, i.e. higher than 18Hz.

Finally, comparing the results obtained on solid pedestal with bust (412_EM_X), Figure 7d and without bust (446_EM_X), Figure 9d, it can be observed that the rocking response of the bust significantly influences that of the solid pedestal, and obviously vice versa.

Different dynamic response was found when the Kalamata-L_X record is considered. The results corresponding to test carried out with the highest value of acceleration, namely 426_KA_X with PGA=0.30g, are shown in Figure 10 through Figure 11. This test was the only one leading to bust overturning. The measured outputs show that the artefact response is significantly affected by the frequency contents of the strong motion. For the Kalamata earthquake a fully developed rocking and overturning were observed for the bust, although the seismic record has horizontal input accelerations lower than Emilia-L in X-direction (412_EM_X), as shown in Table 4. In Kalamata-L_X record a single mainshock can be identified in the time history used as input on the shake table, as illustrated in Figure 6b. The mainshock (between 7s and 10s) possesses multiple cycles with acceleration amplitude exceeding 0.20g and the maximum acceleration is PGA=0.30g. Compared to the Emilia-L_X record used for 412_EM_X, the FFT of the horizontal acceleration time history of Kalamata-L_X input presents large amplifications on lower frequencies, in the range of 0.8-3.5 Hz (Figure 11) in accordance with the higher value of PGV/PGA (Table 3). Two phases can be detected from Figure 10 for the bust response: the first with minor rocking at about 7.2s, and the second with fully developed rocking, leading to overturning. The onset of fully developed rocking motion for the bust is identified through measurements of the gyroscope, at about 8.7s, as well the horizontal acceleration response. The bust oscillations amplify up to the incipient overturning, then they stopped due to external steel cage restraints.

The pedestal follows the vibrations induced by the shaking table; Figure 10a shows a fairly good match of the dynamic response of the pedestal and the table with the presence of multiple high frequency peaks, as can be also seen in Figure 11. The angular velocity in Figure 10b shows that the pedestal is slightly affected by rocking of the bust.

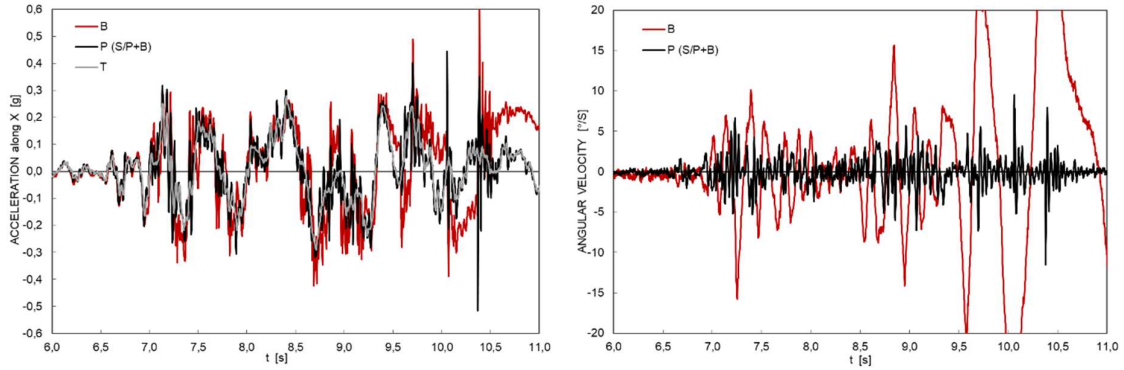

(a) (b)

Figure 10. Test 426_KA_X. (a) Horizontal acceleration: solid pedestal and bust on solid pedestal; (b) angular velocity: solid pedestal and bust on solid pedestal.

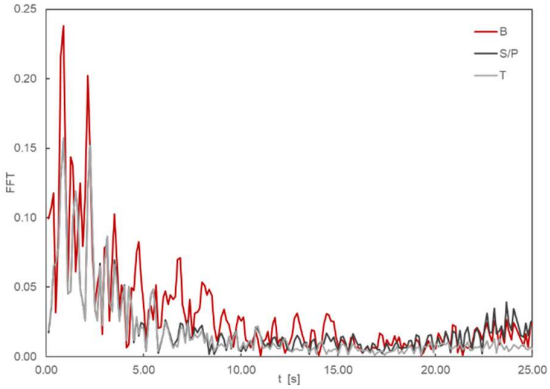

Figure 11. Fast Fourier Transform for the horizontal acceleration signal on shake table (T), solid pedestal (S/P) and bust (B) for test 426_KA_X

Response under biaxial loading

The effects of biaxial loading are discussed with reference to the tests with bidirectional Emilia earthquake horizontal input, 414_EM_XY with a PGA-X=0.34g and PGA-Y=0.25g. The experimental results are shown in Figure 12 and Figure 13 for bust and solid pedestal, respectively. It is found that bust and pedestal continue to vibrate even after the amplitude of the ground motion decreases. The observed response is significantly different form the results in the uniaxial strong motion with similar PGA value, i.e. 402_EM_X, as visible in Sect.3.2 (Figure 17a-b). The occurrence of rocking for the bust, at beginning of the 1st shock, can be identified by the presence of long period (short frequency) response (Figure 12a) as well as by the multiple peaks at high frequencies in the FFT spectrum. Unlike the uniaxial Emilia-L_X inputs (see 412_EM_X), two distinct types of rocking modes caused by the biaxial input can be identified for the bust. A value of rocking period at about 0.2-0.3s can be visually identified for the 1st shock; an increase up to about 0.4s was observed for the 2nd shock. The latter values are confirmed by FFT analysis for the bust dynamic response, where peaks at 2.2, 3.3, 4.2 and 5Hz are found.

The occurrence of rocking motion in the bust can also be detected from the mismatch of the time histories recorded on table and pedestal, as well as their FFT response. Such outcomes can also be found by the time histories of angular velocity and vertical acceleration, Figure 12b-c.

The dynamic behaviour of bust is significantly influenced by biaxial loading in terms of frequency contents.

As far as the solid pedestal is concerned (see Figure 13) it does not exhibit fully developed rocking, but only slight rocking. Also, in this case an increase in high frequency is detected in the measurements of pedestal response, as observed for 412_EM_X.

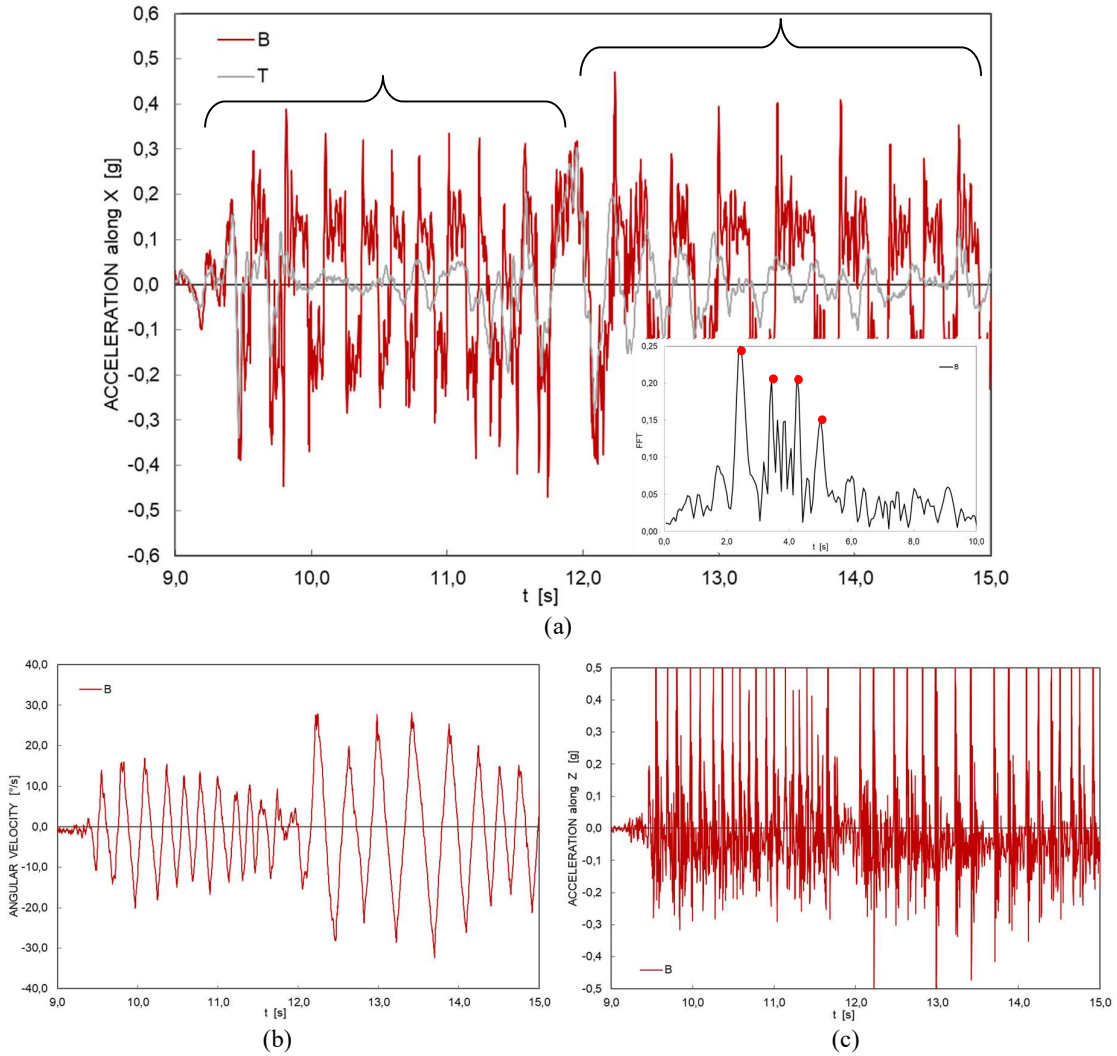

Figure 12. Bust on solid pedestal: 414_EM_XY (a) X-Horizontal acceleration time history with its FFT; (b) X-Angular velocity time history; (c) Vertical acceleration time history.

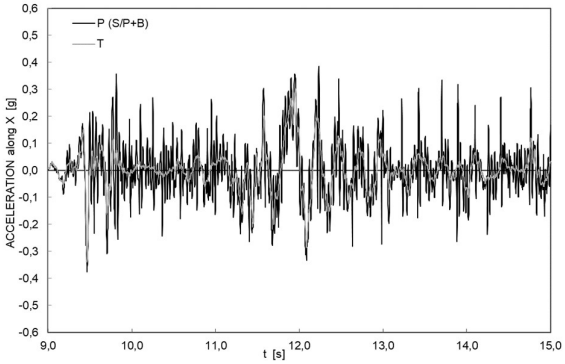

Figure 13. Solid pedestal: 414_EM_XY X-Horizontal acceleration time history.

Considering the Y-direction, the bidirectional input 414_EM_XY has a relatively low PGA value, namely PGA= 0.25g. However, the rocking mode of the bust is activated as shown in Figure 14a. It is worth noting that, for a uniaxial input in Y-direction with a slightly higher PGA (410_EM_Y with PGA=0.30g), the bust does not rock. Additionally, the uniaxial input exhibits lower amplifications of the acceleration for bust than in the biaxial case, as displayed in Figure 14b. The latter findings are confirmed by other similar tests, e.g. 176_EM_XY, PGA,X=0.38g and PGA,Y=0.29g.

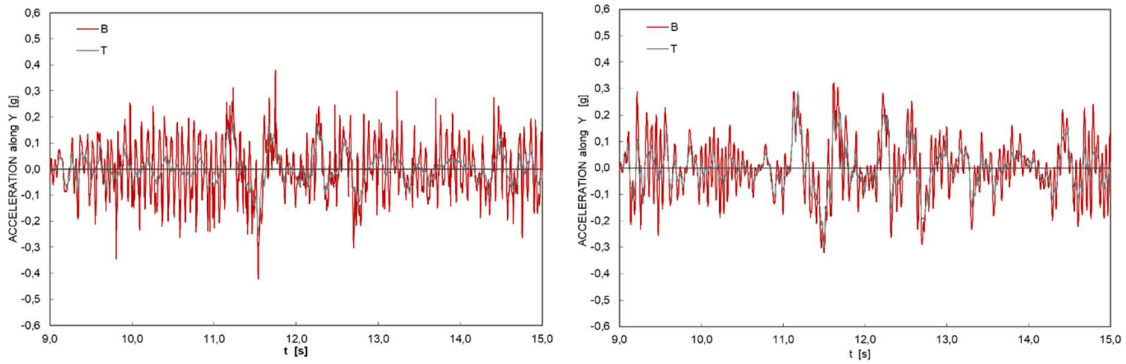

(a) (b)

Figure 14. Horizontal acceleration for table and bust on solid pedestal. (a) 414_EM_XY (b) 410_EM_Y

3.2 Discussion of the observed results

Time histories illustrated in Section 3.1 confirm the complex seismic response of the artefacts tested experimentally via shake table. In the present section, the amplifications recorded for pedestals and busts along with the time gaps between the horizontal acceleration maximum response are considered for further investigations. Table 6 summarizes the outcomes of the horizontal acceleration time history for the solid pedestal and the bust of Augustus for Emilia-L_X and Kalamata-L_X records. The Emilia-L_X strong motion was divided in two shocks (see section 3.1.2) and the acceleration responses were analysed separately for each time interval. Peak values of the accelerations for the three locations along the height of the solid pedestal-bust specimen are reported in bold in Table 6. The occurrence time for each acceleration was also computed. The asynchronous motion may be an indicator for the onset of rocking.

For Emilia 1st shock (between 9s and 11s), the maxima of horizontal accelerations registered on the shake table, pedestal and bust are synchronous. This is not the case for all records in 2nd shock (between 11s and 15s) and for most of the Kalamata records. However, the outcomes of analysis of the measured response parameters demonstrate that there is wobbling of solid pedestal at 1st shock in 407_EM_X and 412_EM_X tests and moreover the visual analyses prove the rocking initiation of bust, for the same tests. A slight rocking was also detected for the solid pedestal at 2nd shock of 446_EM_X. Then it can be concluded that asynchronous motion is not an effective indicator of rocking onset. Moreover, from the comparison of Emilia and Kalamata outcomes, it is found that the time gap between the occurrences of horizontal acceleration maximum response is dependent on the frequency contents of the strong motion.

Table 6. Maximum values of the horizontal accelerations on the shake table, pedestal and bust for Emilia-L_X and Kalamata-L_X records. The values of time when maxima occur have been indicated.

				SHAKE TABLE	SOLID PEDESTAL and AUGUSTUS BUST	
			Occurrence Time (s)	Max ACC_X_T (g)	Max ACC_X_P (g)	Max ACC_X_B (g)
Emilia-L_X	**401**	1st shock	*9,5*	**0,23**	**0,32**	**0,27**
		2nd shock	*11,9*	**0,24**	**0,26**	0,26
			11,5	0,14	0,24	**0,30**
	402	1st shock	*9,4s*	**0,22**	**0,22**	**0,23**
		2nd shock	*11,9*	**0,33**	0,34	0,31
			12,2	0,21	**0,38**	**0,41**
	407	1st shock	*9,4*	**0,35**	**0,48**	**0,50**
		2nd shock	*11,9*	**0,41**	0,40	0,34
			12,3	0,27	**0,59**	**0,74**
	412	1st shock	*9,4*	**0,27**	**0,49**	**0,53**
		2nd shock	*11,9*	**0,47**	0,45	**0,68**
			12,3	0,37	**0,60**	0,36
	446	1st shock	*9,5*	**0,21**	**0,23**	**-**
		2nd shock	*11,9*	**0,48**	**0,49**	**-**

1

			SHAKE TABLE	SOLID PEDESTAL and AUGUSTUS BUST	
		Occurrence Time (s)	Max ACC_X_T (g)	Max ACC_X_P (g)	Max ACC_X_B (g)
Kalamata-L_X	**423**	*7,3*	**0,15**	**0,18**	**0,24**
	424	*7,2*	**0,15**	0,21	**0,36**
		7,8	0,12	**0,22**	0,24
	425	*9,3*	**0,25**	**0,28**	0,26
		7,7	0,13	0,27	**0,33**
	426	*8,7*	**0,30**	0,31	0,42
		11,9s	0.13	**n.a.**	**n.a**

2 Key: n.a. = not applicable as spikes of acceleration were recorded, due to bust overturning

3

4 The amplifications of the horizontal accelerations between the shake table, the pedestals and the busts provide an
5 effective guidance on the levels of forces and displacements experienced by museum artefacts. Such amplifications
6 can be estimated through the coefficient of amplification (CAF) as also suggested in previous work by Di Sarno
7 et al. [36] and Prota et al. [7], which refer to steel free-standing display case/cabinet containing valuable
8 components.
9 Figure 15a shows CAFs of solid pedestal calculated for all earthquakes, including the biaxial input, that range
10 from 1 to 1.8. Therefore, the mean value differs by about 30-80% respectively from the amplification value 1.0
11 for rigid bodies and 2.5 for flexible bodies in the ASCE [54], valid for anchored components. The presence or
12 absence of the bust above the solid pedestal does not change the S/P CAF significantly. Moreover, solid pedestal
13 CAFs are almost independent from PGA and earthquake type, demonstrated by the values in a narrow range.
14 For biaxial input the CAF of solid pedestal does not differ significantly from the monodirectional input, as
15 observed in section 3.1.2. The dynamic response of the hollow pedestal is more complex than the solid counterpart,
16 probably for its greater slenderness. As shown in Figure 15b the CAFs of hollow pedestal range between 1 and 7,
17 and highly vary with both PGA and type of earthquake, i.e. frequency content. CAF can be as high as 7 for Aquila,
18 higher than 5 for Syntagma, and also for Emilia earthquake CAF values of 5.8 can be reached for high PGA values.
19 Even if a clear trend is hardly detectable, CAF tends to grow as PGA increases. When the relationship CAF-PGA
20 is assessed based on "earthquake-to-earthquake" variability, a decrease after an increasing branch can be observed
21 for Emilia, Aquila, Syntagma earthquakes. Such response can therefore be an indicator of rocking system. For the
22 latter records, CAF decrease at about 0.27g. This decrease may be due to a developed rocking in progress.
23 As regards the bust response, the amplification of the bust is on average higher than that of the pedestal. In

particular, Figure 16a shows for Emilia-L_X record that for the bust on solid pedestal CAFs have values between 1.0 and 2.2, while on hollow pedestal CAFs do not follow a clear trend and is highly irregular, as per Figure 16b, denoting the complexity of bust response on Hollow pedestal. In particular, Figure 16b shows the ratio between CAF of hollow pedestal and CAF of solid pedestal for Emilia-L_X record. It can be seen that for low seismicity H/P and S/P amplify about the same, the ratio between them ranges from 0.75 to 1.5; while for PGA > 0.35g the same ratio ranges from 3.0 to 4.25.

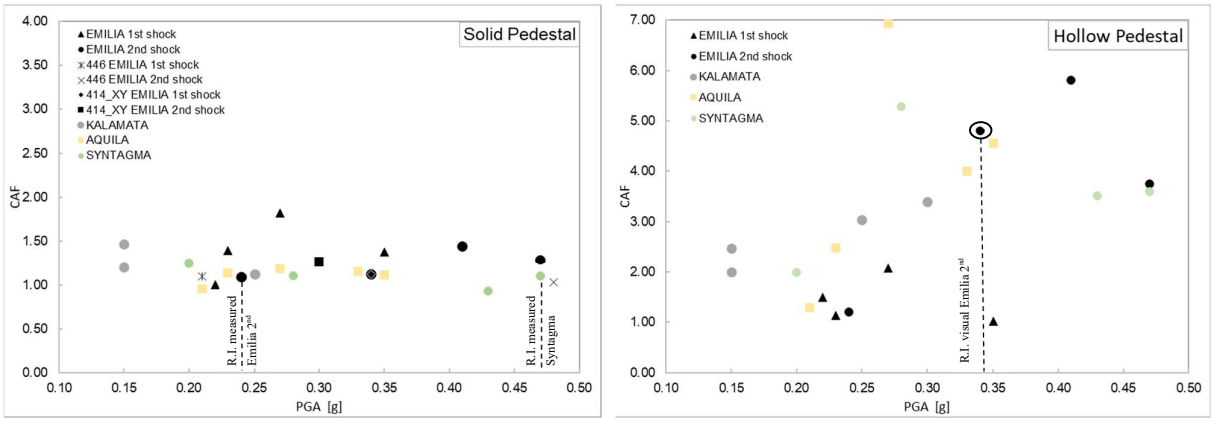

(a) (b)

Figure 15. CAF acceleration values for all earthquakes results: (a) solid pedestal (S/P); (b) hollow pedestal (H/P)

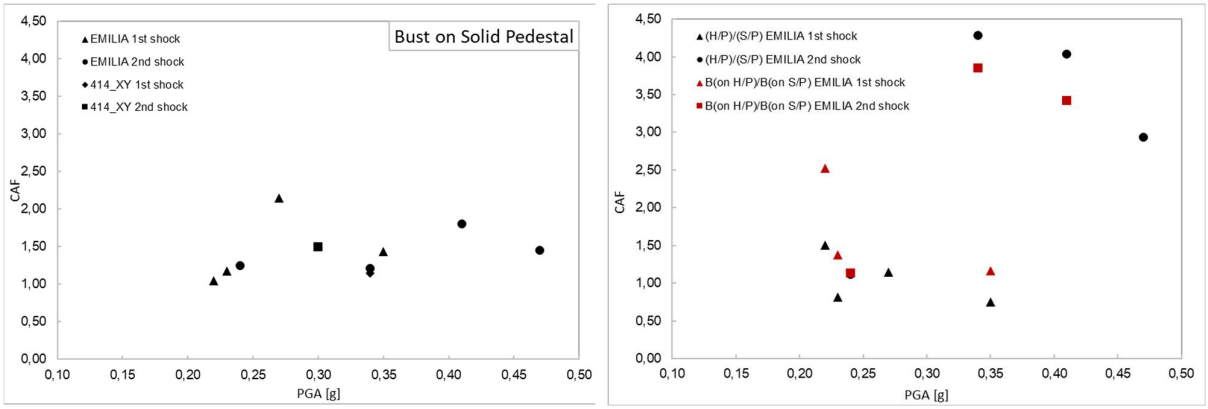

(a) (b)

Figure 16. CAF acceleration of busts for Emilia earthquake tests: (a) CAF values of bust on solid pedestal; (b) ratio between CAF acceleration values of bust on hollow pedestal and bust on solid pedestal

Comparing the above results with the outcomes of visual observation and those from the analysis of the measured response parameters (section 3.1.2), it can be concluded that the analysis of CAFs and of their trend is not an effective indicator of wobbling or rocking motion. For the solid pedestal the variation of CAF with PGA seems insensitive to wobbling or rocking occurrence, detected from the measurements, as visible for Emilia in Figure 15a.

Similar conclusions can be drawn also for hollow pedestal. In this case the presence of a descending branch is not an indicator of rocking initiation, instead it could be an indicator of a fully developed rocking. The outcomes of visual analysis show that in many cases rocking already occurred before the descending branch, as an example in Figure 15b for Emilia earthquake.

The vibration of the pedestal and bust is also monitored through gyroscopes and LVDT, as illustrated in Section 2.3. The angular velocity measured through gyroscopes is effective in determining the onset of rocking and the occurrence of overturning, as well as the pedestal base vertical displacement. The time histories of the angular velocity for solid pedestal and bust are displayed in Figure 17a and Figure 17b respectively when Emilia-L_X records are considered, while Figure 17c-d depict the vertical displacement time history recorded on solid pedestal and on hollow pedestal respectively. In the figures the occurrence time of wobbling and/or rocking initiation is also shown, which has been identified through the analysis of measured response parameters and FFT (as discussed in Section 3.1.2) or directly through visual inspection (Section 3.1.1).

As shown in Figure 17a and Figure 17b the velocity of the pedestal is much lower than the counterpart recorded on the bust. In particular, the bust on solid pedestal reaches peak velocity <5°/s for the tests 401 EM_X, for the tests 407 EM_X and 412 EM_X the angular velocity is higher than 10°/s even for 1st shock and reaches values of about 40°/sec for 2nd shock. For the latter tests, the visual observation clearly identifies the onset of rocking at 1st shock. The response of the solid pedestal in the 1st shock of the tests 407 and 412 leads to angular velocity of about 7.5°/s and, as can be seen in Figure 17c, to LVDT values approaching 0.1mm at most, probably induced by the wobbling due to the imperfections. A similar response is also found for the test 446 in the 2nd shock, where S/P exhibits a slight rocking, with angular velocity close to 8°/s and vertical displacement of 0.1mm.

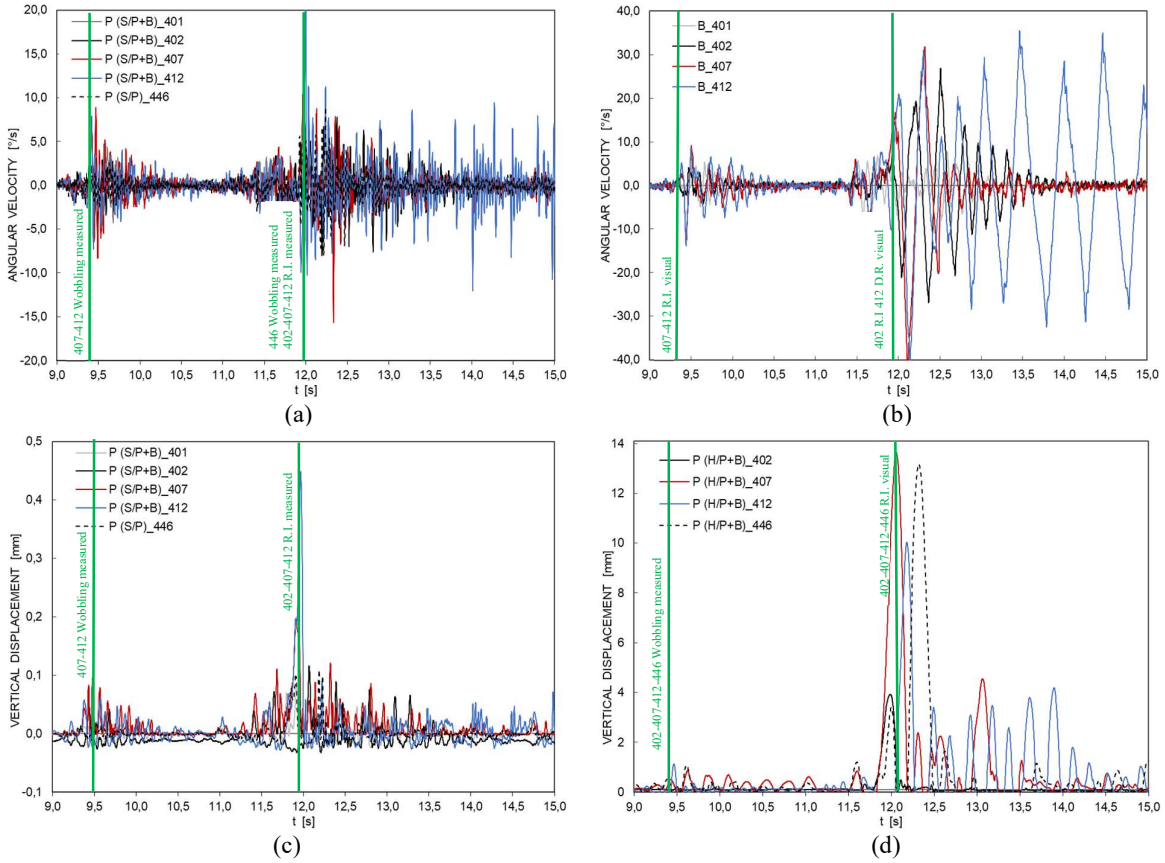

Figure 17. Time history of angular velocity and vertical displacement recorded for Emilia earthquake tests: (a) angular velocity on the solid pedestal; (b) angular velocity on the bust on the solid pedestal; (c) vertical displacement on solid pedestal; (d) vertical displacement on hollow pedestal

Obviously, higher values of angular velocity and LVDT are found for hollow pedestal, indeed angular velocity reaches a maximum of 6°/s (412 EM_X) in 1st shock and then it reaches values even greater than 20°/s in 2nd shock, when also visually rocking motion is observed for all earthquakes (i.e. tests 402 407 412 446). Correspondingly, as recognizable in Figure 17d, the LVDT values of hollow pedestal are much higher than those of the solid one. Actually, it reaches values higher than 10mm when rocking of pedestal is well developed (i.e. all cases except 402 EM_X), and in 1st shock, when wobbling occurs, it exhibits values higher than 0.1mm (even up to 1mm).
The measured values of uplift and of angular velocities are of relevant importance for assessing the rocking response of the object. In particular, in the next section some implications of the experimental results are drown considering the pedestal uplift as engineering demand parameter (EDP). This choice is due to the interest in evaluating the vulnerability of the system, studying it globally. Thus, it is considered appropriate to use a parameter that refers to the base of the system, i.e. LVDT of the pedestal. Further investigations are in progress to assess the correlations between the two parameters (i.e. uplift and angular velocity) and the rocking occurrence. Finally, alternative strategies to estimate the rocking occurrence, based on the use of θ-value derived from angular velocity measurements, are currently being developed by the Authors.

4 Further investigations on the experimental outcomes for the rocking of pedestals

On the basis of the results illustrated in the previous sections, further evaluations were made for the pedestals assuming as initiation of rocking/wobbling a value of LVDT equal to 0.1mm. Figure 18 shows all the results of the tests, grouped by earthquake signal for the different values of PGA registered on the shake table: full markers indicate 'rocking', while empty markers correspond to 'no-rocking'. First and second shock of Emilia earthquake are grouped together. Figure 18a refers to solid pedestal (S/P) and Figure 18b to hollow pedestal (H/P), distinguishing the cases: pedestal alone or pedestal with presence of bust (+B).
It can be noted that H/P is more likely to rocking than the solid counterpart. Actually, the threshold 0.1mm of LVDT is reached even for the lowest values of PGA of the performed tests. Consequently, it is difficult for H/P to assess the PGA value at the initiation of the phenomenon. In other words, the experimental results allow to determine a lower bound of PGA for rocking initiation (LVDT threshold = 0.1 mm) for S/P, but not for H/P.

When the dependence on the earthquakes is considered, for records reproducing Kalamata earthquake, specimens with solid pedestal tend to rock with PGA values lower than they do for Emilia L. This tendency seems to be confirmed by hollow pedestal as well, notwithstanding the above considerations about the absence of a detectable lower bound for PGA of rocking activation. As reported in Sect. 2.4, Kalamata record has higher value of PGV/PGA ratio than the other ground motion records, resulting in different dynamic characteristics, i.e. lower predominant frequencies and longer duration (see also Sect 2.4). The significance of PGV/PGA ratio was also discussed by D'Angela et al. 2021 [24] who emphasised its seismological importance as well as the strong correlation with structural damage. As far as rocking blocks are concerned, PGV/PGA ratio is adopted to identify overturning potentials as suggested in similar works by Purvance et al. 2008 [28], D'Angela et al. 2021 [24] and Berto et al. 2018 [35], among others. The outcomes of the present experimental study show that PGV/PGA may lead to rocking initiation. Figure 19 includes the minimum values of PGV/PGA of tests which lead to rocking for each earthquake record. However, further experimental and numerical investigations are required to corroborate the influence of PGV/PGA ratio on the rocking initiation. Such ratios are also compared in Figure 19 with reference values typically adopted e.g. [52], among many others, to categorize the frequency content and duration of strong motions.
It is worth noting that the seminal work in early 90's by Tso et al. [52] examined the significance of the PGA/PGV ratio to describe the dynamic characteristics of seismic ground motions and their engineering implications. In this study they distinguished 3 ranges of PGA/PGV: low if PGA/PGV < 0.8 g/m/s, high if PGA/PGV > 1.2 g/m/s, and intermediate if the records with 0.8 g/m/s < PGA/PGV < 1.2g/m/s. Such PGA/PGV thresholds were adopted to select reliably the sample earthquake records to assess the rocking mode of rigid blocks in the present experimental work. This complies with the seismic scenario characterized by different peak input energy, as also mentioned in Sect. 2.4.
As shown in Figure 18 S/P tested alone (triangular marker) initiates rocking only in very few cases, for the highest values of PGA. This behaviour is very different from that of the same pedestal with bust above, which oscillates for significantly lower PGA values. It is not possible to confirm this finding also for the H/P, because of the paucity of the results for pedestal alone. In this regard, it is interesting to compare the observed experimental results with the theoretical value a_c of the minimum horizontal acceleration for the onset of rocking. In no-sliding condition this value is conventionally assumed equal to the pseudo-static limit $a_c = B/Hg$, with the meaning of the symbols described in Sect.2.2, as discussed in Berto et al [38].
The shaded area depicted in Figure 18 is delimited by the values a_c evaluated considering the pedestal alone (upper limit $a_{c(P)}$) and the system bust/pedestal (lower limit $a_{c(P+B)}$), using the aspect ratio values reported in Table 1. It can be seen that in presence of bust, both solid and hollow pedestals experience rocking before the value $a_{c(P+B)}$ corresponding to the ideal condition of pedestal moving with the bust like a single rigid body. Therefore, the value $a_{c(P+B)}$ may not be safe for assessing the rocking initiation of pedestal with bust above. Similarly, in case of pedestal alone, the value of $a_{c(P)}$ seems not conservative for hollow pedestal, although such an assumption relies on a reduced number of data as per Figure 18b. It is thus deemed necessary to perform additional experimental tests.
For the sake of comparison Figure 20 shows the results obtained considering the pedestal angular velocity as EDP for rocking occurrence. In particular, basing on the outcomes described in Sect 3.2, a value of the angular velocity equal to 7.5°/s is assumed. It can be observed that, with this assumption, for solid pedestal rocking occurs for PGA values comparable with those found in Figure 18a assuming a LVDT threshold = 0.1 mm. On the other hand, for hollow pedestal rocking motion is experienced for PGA values appreciably higher than those reported in Figure 18b. Thus, the response of solid pedestal in terms of rocking occurrence is less sensitive to the choice of EDP than the hollow pedestal H/P. The experimental outcomes show a clear correlation of solid pedestal with respect to base uplift, while the hollow pedestal has a stronger correlation with angular velocity. However the experimental data are not sufficient to draw final fragility response, which are currently under revision through extensive parametric numerical analyses.

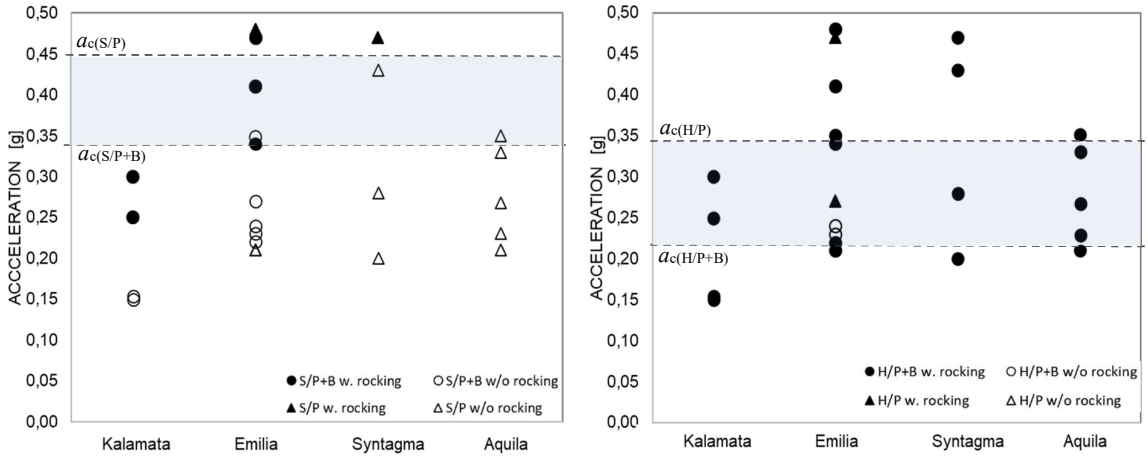

(a) (b)

Figure 18. Rocking indicators for the different PGA values for each earthquake record, for: (a) solid pedestal; (b) hollow pedestal. Rocking was detected assuming threshold equal to pedestal base vertical displacement =0.1mm.

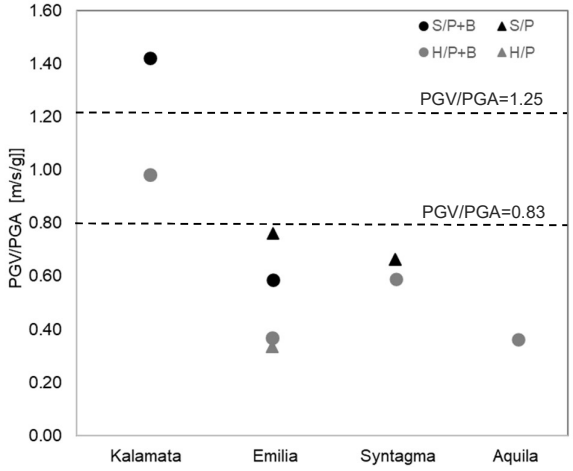

Figure 19. Minimum values of PGV/PGA of signals leading to rocking, both for solid (black) and hollow (grey) pedestals, with and without bust above. Rocking was detected assuming threshold equal to pedestal base vertical displacement = 0.1mm. Dotted lines delimit the PGV/PGA range proposed by Tso et al. [52].

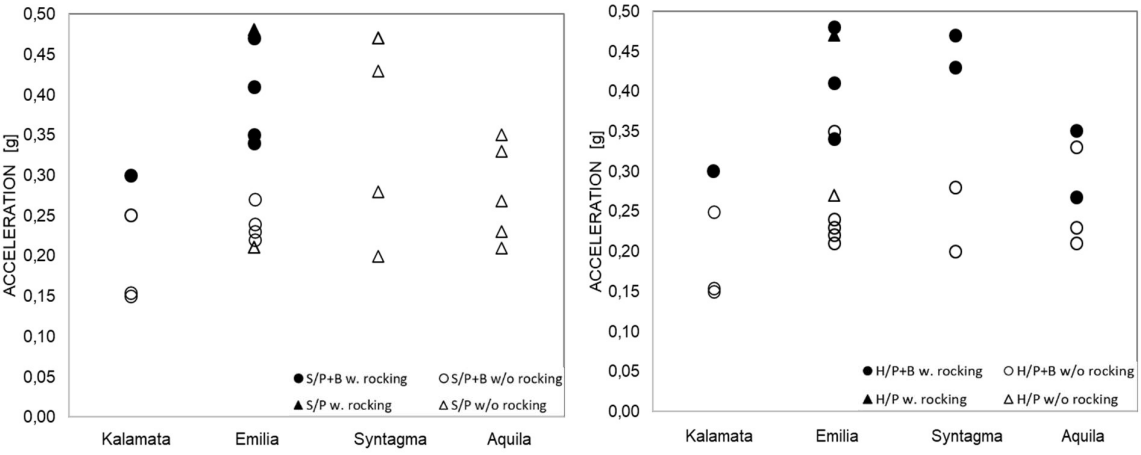

(a) (b)

Figure 20. Rocking indicators for the different PGA values for each earthquake record, for (a) solid pedestal; (b) hollow pedestal. Rocking was detected assuming threshold equal to pedestal angular velocity = 7.5°/s.

5 Conclusions

The present experimental study has focused on the response analysis of museum artefacts consisting of pedestals (solid and hollow) and busts. This study was also aimed at evaluating the reliability of existing simplified formulations to predict the activation of rocking motion. Response parameters such as uplift, horizontal and vertical accelerations, angular velocity were measured to assess the rocking response of the sample busts and pedestals.

The outcomes of the comprehensive shake table tests carried out by using earthquake ground motions with different frequency content showed that uplifts and angular velocity are effective measures for assessing rocking occurrence of tested artefacts. It is also found that the assessment of acceleration time histories measured on the shake table, on the pedestal and bust is not adequate to identify reliably the rocking motion. Indeed, the experimental results discussed in this paper showed that the time gap between the onset of maximum horizontal acceleration on the shake table, on the pedestal and bust is not an effective indicator of rocking occurrence. Similar findings can also be drawn from the relationship between the coefficient of amplification CAF and the PGA, as discussed in detail in section 3.2.

The results of the experimental time history carried out with the shake table considering relatively recent historical records occurred in zones with significant artistic assets highlighted the dependence of the rocking occurrence PGA from the frequency content of the ground motions. For Kalamata record, which has the highest value of PGV/PGA ratio, thus being characterized by lower predominant frequencies and longer duration, solid pedestals tend to rock with PGA values lower than those correspondent to the other ground motion records.

The coefficient of amplification (CAF) of acceleration, which provides an effective guidance on the levels of forces experienced by the artefacts, was also computed for experimental tests carried out on busts and pedestals. The computed values showed that: for solid pedestal CAFs range from 1 to 1.8 and are almost independent from PGA and earthquake type. For Hollow pedestal the CAFs range between 1 and 7; they depend significantly on both PGA and earthquake characteristics. For the busts, the amplification of the acceleration is on average higher than that of the pedestal. For the bust on solid pedestal, CAFs have values between 1.0 and 2.2. There is not a clear trend for the CAF on hollow pedestal. It is also found that, for low seismicity, H/P and S/P show a similar amplification (the ratio between them ranges from 0.75 to 1.5), while for PGA > 0.35g the same ratio ranges from 3.0 to 4.25. Due to the more comparable weight of H/P to the upper bust weight respect to the S/P, H/P is remarkably influenced by the dynamic of the bust. For this reason, the H/P dynamic itself is rather complex and must be further investigated.

Considering the theoretical value $a_c = B/Hg$ of the minimum horizontal acceleration for the onset of rocking it is found that such value is not conservative for the identification of rocking initiation of pedestal with bust above.

The assessment of experimental data discussed in the present paper has also emphasized the paucity of existing data which require urgent future investigations to estimate reliably the risk assessment of museum artefacts. The effects of frequency contents of ground motions and its combination with PGA, as well as the correlations between uplift and angular velocity with rocking occurrence, require additional experimental and numerical studies, aimed at characterizing the threshold limits of response parameters and deriving robust fragility relationships for museum artefacts. Finally, it is recommended to obtain further data through the monitoring of museum artefacts during the earthquakes and collecting information from ground-borne vibrations, e.g. micro-tremors. Such an approach can be implemented through installation of minute sensors and data crowd-sourcing of visitors.

6 Acknowledgments

The financial support of the “Seismology and Earthquake Engineering Research Infrastructure Alliance for Europe” (SERA) (European Commission, H2020-INFRAIA-2016-2017, Agreement No.730900) to the project “Seismic Resilience of Museum Contents” (SEREME) is greatly acknowledged. Any opinions, findings and conclusions, or recommendations expressed in this paper are those of the authors and do not necessarily reflect those of SERA sponsors. The PON MIUR project “GEstioNE del rischio SISmico per la valorizzazione turistica dei centri storici del Mezzogiorno (GENESIS)” (ARS01_00883- CUP D96G18000160005), is also greatly acknowledged.

7 References

[1] Caliò I, Marletta M. Passive control of the seismic rocking response of art objects. *Eng Struct* 2003;25:1009–18. doi:10.1016/S0141-0296(03)00045-2

[2] Lowry M, Armendariz D, Farra BJ, Podany J. Seismic mount making: a review of the protection of objects in the J. Paul Getty Museum from earthquake damage. *Advances in the protection of museum collections from earthquake damage symposium* held at the J. Paul Getty Museum at the Villa on May3–4, 2006. Los Angeles: J. Paul Getty Museum Trust; 2008. p. 45–70.

[3] Berto L, Favaretto T, Saetta A, Antonelli F, Lazzarini L. Assessment of seismic vulnerability of art objects: The “Galleria dei Prigioni” sculptures at the Accademia Gallery in Florence. *J Cult Herit* 2012;13(1)7-21. doi:10.1016/j.culher.2011.06.005. doi: 10.1016/j.culher.2011.06.005

[4] Berto L, Favaretto T, Saetta A. Seismic risk mitigation technique for art objects: experimental evaluation and numerical modelling of double concave curved surface sliders", *Bull Earthq Eng* 2013; 11(5), 1817-1840. doi:10.1007/s10518-013-9441-8
[5] Lagomarsino S, Cattari S. PERPETUATE guidelines for seismic performance-based assessment of cultural heritage masonry structures. *Bull Earthq Eng* 2015;13(1):13–47. doi:10.1007/s10518-014-9674-1
[6] Baggio S, Berto L, Rocca I, Saetta A. Vulnerability assessment and seismic mitigation intervention for artistic assets: from theory to practice. *Eng Struct* 2018;167(1):272–286. doi:10.1016/j.engstruct.2018.03.093
[7] Prota A, Zito M, D'Angela D, Toscano G, Ceraldi C, Fiorillo A, Magliulo G. Preliminary Results of Shake Table Tests of a Typical Museum Display Case Containing an Art Object, *Adv Civ Eng* 2022; (1-18), doi:10.1155/2022/3975958.
[8] Palermo A, Pampanin S, Marriott D. Design, modeling, and experimental response of seismic resistant bridge piers with posttensioned dissipating connections. *J Struct Eng* 2007; 133(11):1648–1661. doi: 10.1061/(ASCE)0733-9445(2007)133:11(1648)
[9] Cheng C. Shaking table tests of a self-centering designed bridge substructure. *Eng Struct* 2008; 30(12):3426–3433. doi:10.1016/j.engstruct.2008.05.017
[10] Di Sarno L., Del Vecchio C., Maddaloni G., Prota A. Experimental response of an existing RC bridge with smooth bars and preliminary numerical simulations. *Eng Struct* 2017; 136, 355-368. doi:10.1016/j.engstruct.2017.01.052.
[11] Housner GW. The behavior of inverted pendulum structures during earthquakes. *Bull Seismol Soc Am* 1963; 53(2):403–417. doi:10.1785/BSSA0530020403
[12] Ishiyama Y, Motion of rigid bodies and criteria for overturning by earthquake excitations, *Earthq Eng Struct Dyn* 1982; 10(5)630–650. doi:10.1002/eqe.4290100502
[13] Zhang J, Makris N. Rocking response of free-standing blocks under cycloidal pulses, *J Eng Mech* 2001; 127(5):473-483. doi:10.1061/(ASCE)0733-9399(2001)127:5(473).
[14] Voyagaki E, Psycharis IN, Mylonakis G, Rocking response and overturning criteria for free standing rigid blocks to single—lobe pulses, *Soil Dyn. Earthq. Eng.* 2013; 46(2):85-95. doi: 10.1016/j.soildyn.2012.11.010.
[15] DeJong M and Dimitrakopoulos E. Dynamically equivalent rocking structures. *Earthq Eng Struct Dyn* 2014; 45(10), 1543-1563. doi:10.1002/eqe.2410
[16] Dimitrakopoulos EG and Paraskeva TS. Dimensionless fragility curves for rocking response to near-fault excitations, *Earthq Eng Struct Dyn* 2015; 44(12):2015–2033. doi:10.1002/eqe.2571
[17] Dimitrakopoulos EG and Fung EDW. Closed-form rocking overturning conditions for a family of pulse ground motions. *Proc R Soc A* 2016. 4722016066220160662, doi:10.1098/rspa.2016.0662.
[18] Diamantopoulos S and Fragiadakis M. Seismic response assessment of rocking systems using single degree-of-freedom oscillators. *Earthq Eng Struct Dyn* 2019; 48 (7) 689-708. doi:10.1002/eqe.3157.
[19] Fragiadakis M and Diamantopoulos S. Fragility and risk assessment of freestanding building contents, *Earthq Eng Struct Dyn* 2020; 49 (10):1028–1048. doi:10.1002/eqe.3276
[20] Diamantopoulos S and Fragiadakis M. Modeling, fragility and risk assessment of ancient freestanding columns and colonnades, *Eng Struct* 2023; doi:10.1016/j.engstruct.2022.115273.
[21] Yim CS, Chopra AK, Penzien, J. Rocking response of rigid blocks to earthquakes. *Earthq Eng Struct Dyn* 1980; 8: 565-87. doi:10.1002/eqe.4290080606
[22] Spanos PD, Koh A. Rocking of rigid blocks due to harmonic shaking. *J Eng Mech* 1984; 110(11):1627–1643.
[23] Arredondo CA, Reinoso E. Influence of Frequency Content and Peak Intensities in the Rocking Seismic Response of Rigid Bodies, *Journal of Earthquake Engineering* 2008; 12: 517–533. doi.org/10.1080/13632460701672755
[24] D'Angela D, Magliulo G, Cosenza E. Towards a reliable seismic assessment of rocking components, *Engineering Structures* 2021; 230, doi.org/10.1016/j.engstruct.2020.111673
[25] Milne J. Seismic experiments. *Trans Seism Soc Japan* 1885; 8:1–82. doi:10.1061/(ASCE)0733-9399(1984)110:11(1627)
[26] Milne J, Omori F. On the overturning and fracturing of Brick and other Columns by horizontally applied Motion. *Seismol J Jpn* 1893; 17:59–86.
[27] Kirkpatrick P. Seismic measurements by the overthrow of columns. *Bull Seismol Soc Am* 1927; 17, 95–109. doi:10.1785/BSSA0170020095
[28] Purvance MD, Anooshehpoor A, Brune JN. Freestanding block overturning fragilities: numerical simulation and experimental validation. *Earthq Eng Struct Dyn* 2008; 37, 791–808. doi:10.1002/eqe.789
[29] Konstantinidis D, Makris N. Experimental and analytical studies on the response of freestanding laboratory equipment to earthquake shaking. *Earthq Eng Struct Dyn*. 2009; 38:827-848. doi:10.1002/eqe.871
[30] Berto L, Bovo M, Rocca I, Saetta A, Savoia M. Seismic safety of valuable non-structural elements in RC buildings : Floor Response Spectrum approaches. *Eng Struct*. 2020; 205:110081. doi:10.1016/j.engstruct.2019.110081
[31] Petrone C, Magliulo G, Manfredi G. Floor response spectra in RC frame structures designed according to Eurocode 8. *Bull Earthq Eng* 2016;14(3):747–67. doi:10.1007/s10518-015-9846-7.

[32] Rodriguez, D, Perrone, D, Filiatrault, A. Seismic demand on non-structural elements for quantifying seismic performance factors. *Earthquake Engng Struct Dyn*. 2022; 1-24. doi:10.1002/eqe.3799
[33] Kafle B, Lam NT, Gad EF, Wilson J. Displacement controlled rocking behaviour of rigid objects. *Earthq Eng Struct Dyn*. 2011, 40:1653–1669. doi:10.1002/eqe.1107
[34] Petrone C, Di Sarno L, Magliulo G, Cosenza E. Numerical modelling and fragility assessment of typical freestanding building contents. *Bull Earthq Eng* 2017; 15:1609–33. doi:10.1007/s10518-016-0034-1.
[35] Berto L, Rocca I, Saetta A. Vulnerability assessment methods for rocking and overturning of free standing elements. *Soil Dyn Earthq Eng* 2018; 110. doi:10.1016/j.soildyn.2018.02.010.
[36] Di Sarno L, Magliulo G, D'Angela D, Cosenza E. Experimental assessment of the seismic performance of hospital cabinets using shake table testing. *Earthq Eng Struct Dyn* 2019; 48(1), 103-123. doi:10.1002/eqe.3127
[37] D'Angela D, Magliulo G, Cosenza E. Seismic damage assessment of unanchored nonstructural components taking into account the building response. *Structural Safety* 2021, 93, Article ID 102126. doi:10.1016/j.strusafe.2021.102126
[38] Berto L, Meroi E, Rocca I, Saetta A. Rocking activation of free standing elements in real conditions: a safe experimentally-based acceleration limit. *Eng Struct* 2021; 226. doi:10.1016/j.engstruct.2020.111331.
[39] Wittich CE and Hutchinson TC. Shake table tests of unattached, asymmetric, dual-body systems. *Earthq Eng Struct Dyn*. 2017. 46(9) 1391-1410. doi:10.1002/eqe.2860
[40] Arredondo C, Jaimes MA, Reinoso E. A simplified model to evaluate the dynamic rocking behavior of irregular free-standing rigid bodies calibrated with experimental shaking-table Tests. *J Earthq Eng* 2019; 23, 46–71. doi:10.1080/13632469.2017.1309601
[41] Al Abadi H, Paton-Cole V, Gad E, Lam N, Patel V. Rocking Behavior of Irregular Free-Standing Objects Subjected to Earthquake Motion, *J Earthq Eng.* (2019), 23:5, 793-809, doi: 10.1080/13632469.2017.1342305.
[42] Khalid Saifullah M, Wittich C.E., Seismic Response of Two Freestanding Statue-Pedestal Systems during the 2014 South Napa Earthquake, *Journal of Earthquake Engineering* (2021), 26:10, 5086-5108. https://doi.org/10.1080/13632469.2020.1859004
[43] Anagnostopoulos S, Norman J, Mylonakis G. Fractal-like overturning maps for stacked rocking blocks with numerical and experimental validation. *Soil Dynamics and Earthquake Engineering* (2019), 125, [105659]. https://doi.org/10.1016/j.soildyn.2019.04.033
[44] Casapulla C, Giresini L, Lourenço P.B. Rocking and kinematic approaches for rigid block analysis of masonry walls: state of the art and recent developments. *Buildings* 2017, 7, 69. doi:10.3390/buildings7030069
[45] https://sera-ta.eucentre.it/
[46] Fragiadakis M, Di Sarno L, Saetta A, Castellano MG, Rocca I, Diamantopoulos S, Crozet V, Politopoulos I, Chaudat T, Vasic S, Bal IE, Smyrou E, Psycharis I, Hutchinson TC, Berto L. *D10.1 - Technical report on SERA Transnational access activities TA1-TA10 M36* – SEREME Seismic Resilience of Museum contents. 2020.
[47] Ambraseys N, Psychiaris I. Earthquake stability of columns and statues. *J Earthq Eng.* 2011; 15(5). 685-710. doi:10.1080/13632469.2010.541549
[48] Shenton HW, Jones NP, Base excitation of rigid bodies. I: formulation, *J Eng Mech (ASCE)* 1991; 117 (10) 2286–2306. doi:10.1061/(ASCE)0733-9399(1991)117:10(2286)
[49] Drosos V, Anastasopoulos I. Shaking table testing of multidrum columns and portals. *Earthq Eng Struct Dyn* 2014; 43, 1703–1723. doi:10.1002/eqe.2418
[50] Wittich CE, Hutchinson TC. Shake table tests of stiff, unattached, asymmetric structures. *Earthq Eng Struct Dyn* 2015; 44, 2425-2443. doi:10.1002/eqe.2589
[51] https://www.faro.com/it-IT/Products/Hardware/Focus-Laser-Scanners
[52] Tso WK, Zhu TJ, Heidebrecht. Engineering implication of ground motion A/V ratio. *Soil Dyn. Earthq. Eng.* 1992; 11. 133-144. doi:10.1016/0267-7261(92)90027-B.
[53] Elnashai A, Di Sarno L. *Fundamentals of earthquake engineering*. Chichester: John Wiley and Sons; 2015. doi:10.1002/9780470024867
[54] ASCE/SEI Standard 7−10. Minimum design loads for buildings and other structures. *Reston, VA: American Society of Civil Engineers*; 2010. doi:10.1061/9780784412916